Behavior of Unbonded, Post-Tensioned, Precast Concrete Connections with Different Percentages of Mild Steel Reinforcement

Sevket Ozden, Ph.D.
Assistant Professor
Department of Civil Engineering
Kocaeli University
Kocaeli, Turkey

Onur Ertas
Research Assistant
Department of Civil Engineering
Bogazici University
Bebek, Istanbul, Turkey

This paper presents the results of tests performed on post-tensioned, precast concrete moment-resisting, beam-column connections containing different mild steel reinforcement contents. In the experimental program, five hybrid connections were tested under displacement-controlled reversed cyclic loading. The main variable was the mild steel's percentage of contribution to the flexural capacity of the connection, ranging from 0% to 65% of the connection's moment capacity. Each hybrid connection was compared with the test result of the reference monolithic subassembly in terms of connection strength, stiffness degradation, energy dissipation, and permanent displacement. The objective of this study was to determine the effect of mild steel reinforcement content on the behavior and performance of post-tensioned, precast concrete hybrid connections. The response of post-tensioned, precast concrete hybrid connections approached that of the monolithic subassembly as the mild steel reinforcement content increased. Connection capacities were well predicted by the joint gap-opening approach. The design assumptions of hybrid connections are best satisfied with a 30% mild steel reinforcement contribution to the connection's flexural capacity.

Although precast concrete construction provides high-quality structural members, the performance of the overall structural system is mostly governed by the capacity of the connections. A properly designed and detailed beam-to-column connection should be able to transfer forces between precast concrete elements, even when subjected to occasional overloads. According to Englekirk,[1] the concept of properly designed connection was expected to do the following:

- Avoid extensive welding;
- Incorporate adequate tolerances for assembly;

- Avoid large, formed wet joints; and
- Minimize crane time with proper joint detailing.

Post-earthquake field investigations of precast concrete structures after the 1999 Kocaeli and Duzce earthquakes in Turkey revealed that the damage and performance of the buildings were closely related to the performance of the connections. As a result, a two-phase research program on the performance of ductile beam-column connections of precast concrete elements was developed at the Bogazici and Kocaeli universities following the 1999 earthquakes.

This research program is funded by the Scientific and Technical Research Council of Turkey (TUBITAK-Project No. ICTAG I589) and the Turkish Precast Concrete Association. Phase I of the study focused on the performance of composite, bolted, and cast-in-place concrete connections[2] while phase II mainly dealt with the performance of post-tensioned, precast concrete connections containing various levels of mild steel reinforcement. This paper presents the experimental observations from phase II of the research program. All connections in this research program were detailed according to ACI T1.2-03.[3]

LITERATURE SURVEY

The performance of post-tensioned, precast concrete connections has been the subject of considerable research in the past two decades. The location of prestressing tendons, the level of post-tensioning force, and the use of bonded or unbonded tendons were the main variables in the available literature. In the study of Park and Thomson,[4] 10 nearly full-scale beam-to-interior-column precast concrete subassemblies were tested with different proportions of prestressing tendon area to non-prestressed steel area. These tests showed that the ductility of the pre-stressed concrete beams could be enhanced with the presence of non-prestressed reinforcement in the compression zones. A central prestressing tendon at mid-depth of the beam,

which passed through the joint, was shown to be effective in contributing to the joint's core shear strength. Moreover, the analytical study revealed that the introduction of a prestressing tendon at mid-depth of a concrete section that was reinforced equally on top and bottom with non-prestressing steel increased the cracking and flexural strengths of the section without significantly reducing its ductility.[5]

Different types of precast concrete connections, of which three were post-tensioned or composite connections with post-tensioning, were tested by French et al.[6,7] It was reported that failures were observed either inside or outside of the connection region for the post-tensioned concrete specimens. The strength and energy dissipation characteristics of the connections were adequate with respect to monolithic specimens regardless of the location of failure.

In the research of Palmieri et al.,[8] two types of connections were designed based on nonlinear elastic post-tensioning concepts. The main difference between specimens (UMn-PTS and UMn-PTB) was the member size and post-tensioning type. Furthermore, a third connection (UT-PTS) was designed with pre-tensioning instead of post-tensioning. It was reported that the prestressed concrete specimens exhibited the desired nonlinear elastic behavior through the 3% drift level.

In the development of a moment-resisting precast concrete connection with post-tensioning, a multiyear research program was developed by the National Institute of Standards and Technology (NIST). In phase I of the experimental program, monolithic and post-tensioned precast concrete subassemblies were tested. The post-tensioning bars were fully grouted in this phase of the study.[9] As a result of the low energy dissipation observed in the precast concrete specimens of phase I, several methods for increasing the energy dissipation capacity of the precast concrete connections were explored in phase II. These methods include changing the location of the post-tensioning steel and using prestressing strands instead of post-tensioning bars.[10]

Zero slope hysteresis loops were ob-

served upon load reversal in both the phase I and phase II tests of the NIST research. The subassemblies suffered excessive stiffness degradation and slip at low displacements. It was concluded that such stiffness degradation was mainly caused by a reduction in the effective clamping force developed by the prestressing bars.[10] Because the prestressing bars of the phase I and phase II specimens were fully grouted, the plastic deformation of the bars was forced to short bar lengths, resulting in strains beyond the bar proportional limits and even beyond the ultimate limit.

The required ultimate displacement of the subassembly could be achieved without exceeding the proportional limit of the prestressing steel by choosing correct debonded bar lengths, an option that also solved the problem of the zero slope hysteresis loops.[11] This concept of correct debonded bar length was applied in phase III of the NIST research, and the specimens did not exhibit zero stiffness upon load reversals.[10]

In phase IV of the NIST research, post-tensioned, precast concrete connections with mild steel reinforcement were studied. In these connections, the mild steel reinforcement and the pre-stressing tendons contributed to the connection moment capacity. It was concluded that the use of bonded mild steel reinforcement at the top and bottom of the cross section, along with the use of unbonded prestressing tendons, resulted in the most practical combination in the response of the subassembly.[12] Phase IV tests also demonstrated that hybrid connections were self-centering and displayed essentially no residual drift.

Two ungrouted, post-tensioned, precast concrete beam-to-column joint subassemblies were tested by Priestley and MacRae.[13] One of the subassemblies represented an exterior joint, while the other represented an interior joint. It was reported that the structural response of both specimens was satisfactory, despite the very low levels of reinforcement provided in the beams, columns, and joints.

The objective of the Precast Seismic Structural Systems (PRESSS) research program was to develop an effective
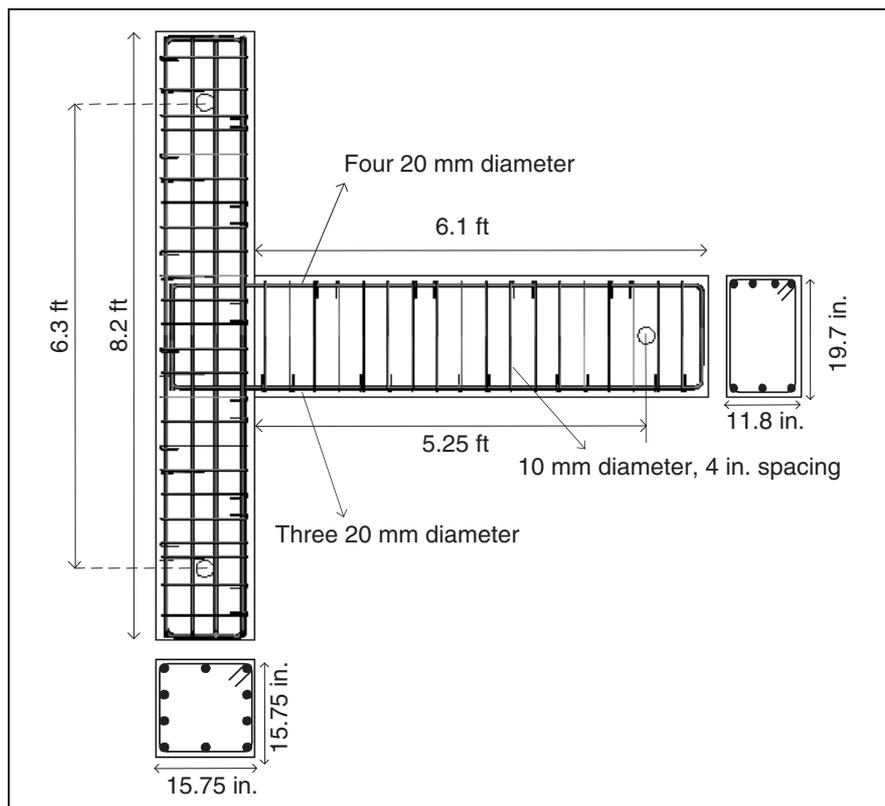
Fig. 1. Dimensions and reinforcement detail of monolithic specimen M. Note: 1 in. = 25.4 mm; 1 ft = 0.3048 m.

seismic structural system for precast concrete buildings in order to reduce building costs through rapid site erection and low labor requirements.[14] As part of this program, a 60% scale five-story precast concrete building was tested under pseudo-dynamic test procedures at the University of California at San Diego (UCSD). The major objective of the test was to develop design guidelines for precast/prestressed concrete seismic systems.[15,16]

The building comprised four different ductile structural frame systems in one direction of response and a jointed structural wall system in the orthogonal direction. The seismic frame connection types were hybrid post-tensioned, pretensioned, tension-compression yield (TCY)–gap, and TCY connections. It was reported that the behavior of the structure was extremely satisfactory. Damage to the building in the frame direction of response was much less than the expected damage for an equivalent reinforced cast-in-place concrete structure. On the other hand, the beams of the hybrid frames experienced some torsion about the longitudinal axes during testing.[16]

TEST SPECIMEN AND CONNECTION DETAILS

Phase II test specimens of the current study were modeled as exterior joints of a multistory building. The monolithic reinforced concrete specimen was designed according to the strong-column weak-beam design philosophy for high seismic regions, while the design of post-tensioned, precast concrete connections was based on both the ACI T1.2-03 design guidelines and the recommendations and conclusions from previously published research. All test specimens were scaled to approximately half of the prototype structure in geometry.

As a result, the cross-sectional dimensions of the beam were 11.8 in. × 19.7 in. (300 mm × 500 mm) and the clear span of beam was 5.25 ft (1.6 m). Hence, the shear-span-to-height ratio (a/h) was about 3.2. The height of the column was 6.3 ft (1.9 m), and it had a square cross section with 15.75 in. (400 mm) dimensions. The cover thickness in the precast concrete beam and column was 0.8 in. (20 mm). The dimensional and rein-

forcement details of the subassembly are given in **Fig. 1**.

Monolithic Specimen

The monolithic reinforced concrete specimen (M) was designed according to the requirements for high seismic zones. The longitudinal reinforcement ratio in the columns for specimen M and also for the post-tensioned, precast concrete specimens was 2%. Along the column height, including the joint region, the spacing of closed stirrups was approximately 4 in. (100 mm). The beam's flexural reinforcement consists of four 0.8-in.-diameter (20 mm) and three 0.8-in.-diameter reinforcing bars placed at the top and the bottom of the beam, respectively (Fig. 1). The bottom reinforcement of the beam was less than the top reinforcement due to the effects of gravity for a continuous beam.

For all test specimens, monolithic and precast concrete, the same grade of steel was used for the longitudinal and lateral reinforcement. The nominal diameter of the reinforcing steel for the longitudinal and transverse reinforcement was 0.8 in. (20 mm) and 0.4 in. (10 mm), respectively. Yield and ultimate strengths of the 0.8-in.-diameter reinforcing bars were 68.5 ksi (472 MPa) and 83.3 ksi (574 MPa), respectively, while these values for the 0.4-in.-diameter transverse reinforcement were 72.5 ksi (500 MPa) and 81.2 ksi (560 MPa), respectively. Elongation of the reinforcing steel at ultimate strength was 14% for the 0.8-in.-diameter bar and 13% for the 0.4 in. bar. The compressive strength of the concrete for specimen M was 5801 psi (40 MPa).

Post-Tensioned, Hybrid Precast Concrete Connections

All of the precast concrete beams and columns were produced in a precast concrete manufacturing facility. The main variable investigated in the post-tensioned, precast concrete specimens was the mild steel reinforcement content in the connection region. In the first precast concrete specimen, no mild steel reinforcement was used in the connection and the flexural moment

was carried solely by the prestressing strands. This specimen was designated PTM0.

For the second precast concrete specimen, PTM10, the contribution of mild steel reinforcement to the flexural moment capacity was 10%. This 10% ratio is the minimum level of mild steel reinforcement in precast concrete connections stated in the Turkish *Building Code Requirements for Prestressed Concrete (TS3233)*[17] and *Specifications for Structures to Be Built in Disaster Areas*.[18] The mild steel reinforcement contribution to flexure was increased to 30% (specimen PTM30) and 50% (specimen PTM50) in the third and fourth precast concrete connection designs, respectively.

The fourth specimen (PTM50) met the upper limit for mild steel reinforcement contribution to flexural capacity according to ACI T1.2-03 design guidelines. In the fifth and last precast concrete specimen, the mild steel reinforcement contribution to the flexural capacity of the connection was 65% (specimen PTM65), exceeding the upper limit of ACI T1.2-03 design recommendations.

The geometry and reinforcement details of the precast concrete beams, except for specimen PTM0, were the same (**Fig. 2**). All precast concrete beams had a blockout channel at the top and the bottom of the cross section to allow installation of mild steel reinforcement during the assembly process. The length of the channel was 39.4 in. (1000 mm), with cross-sectional dimension of 5.8 in. × 3.9 in. (150 mm × 100 mm). Also, there was a polyvinyl chloride (PVC) pipe with a 3.9 in. (100 mm) inner diameter at the center of the beam cross section for installation of the prestressing strands. Four 0.8-in.-diameter (20 mm) mild steel reinforcing bars were placed at the top and bottom of the precast concrete beam as main longitudinal reinforcement. The detail is shown in Fig. 2.

The cross-sectional dimensions of the precast concrete beams in the connection region were the same as those of the monolithic specimen. For the precast concrete members (beams and columns), rectangular steel boxes were installed in the connection region as illustrated in **Fig. 3**. Boxes were used
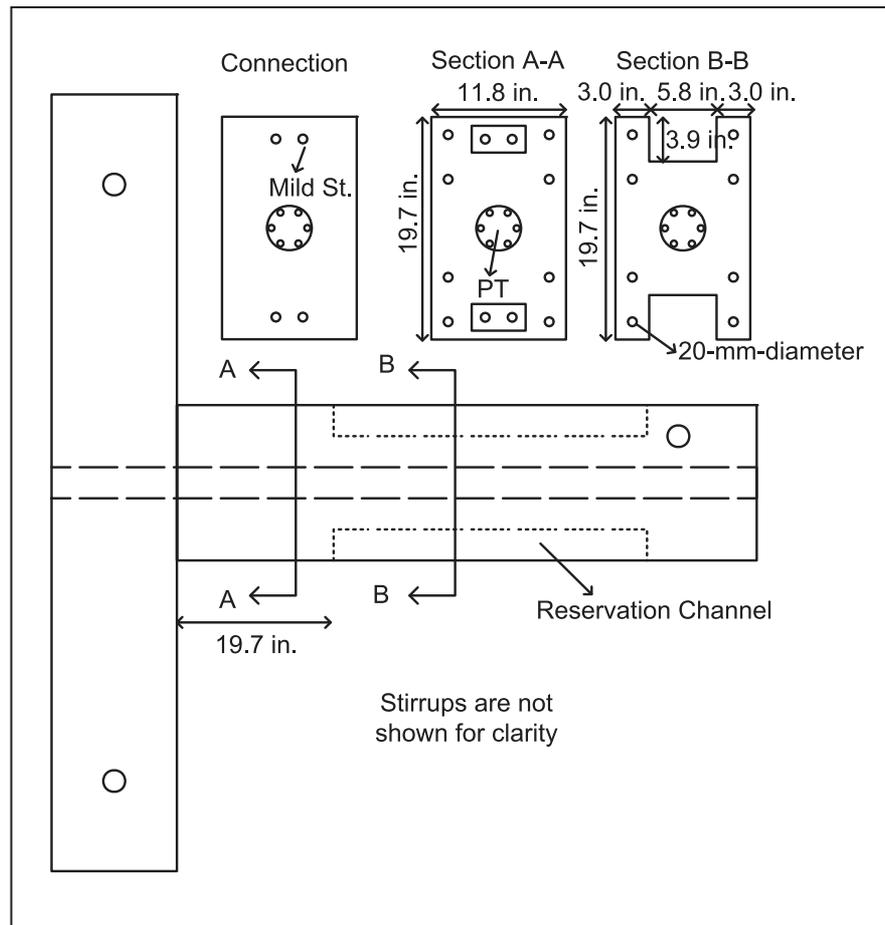
Fig. 2. Details of post-tensioned specimens. Note: 1 in. = 25.4 mm.

instead of pipes to create more dimensional tolerance to compensate for potential production errors and to reserve adequate space for multiple mild steel reinforcing bars.

The 19.7-in.-long (500 mm) rectangular steel boxes installed at the connection region had cross-sectional dimensions of 4.7 in. × 2.35 in. (120 mm × 60 mm) and were located along the same axes on the beam and the column. To prevent the steel boxes from sliding relative to the beam concrete, steel rods, which served as ribs, were welded around the boxes. In addition, steel anchors passing through the box cross section were installed to prevent any possible sliding of the infill grout with respect to the steel box (Fig. 3).

Steel plates were placed at the top and bottom of the beam cross section at the connection region to minimize crushing of the beam concrete. The steel plates were connected to each other by welding two 0.4-in.-diameter (10 mm) reinforcing bars to the plates. The steel plates were also anchored to the beam

concrete. In this beam end region, closed stirrups were installed with an on-center spacing of 2.8 in. (70 mm).

Initially, in the assembly process, the 0.6 in. (15 mm) gap between the precast concrete beam and the column was filled with a self-leveling, nonshrink grout with a compressive strength of approximately 8700 psi (60 MPa). After 24 hours of grout curing time, mild steel reinforcing bars were placed through the steel boxes and the threaded ends were hand tightened. To determine when the mild steel reinforcement would yield during the test, strain gauges were attached to the bars.

Steel plates were placed on both ends of the steel boxes (as washers), and the mild steel reinforcing bars were locked with nuts to prevent slipping (**Fig. 4**). The steel boxes were then filled with the same self-leveling, nonshrink grout. Finally, 0.5-in.-diameter (13 mm) prestressing strands with an ultimate strength of 270 ksi (1860 MPa) were placed at mid-depth of the beam
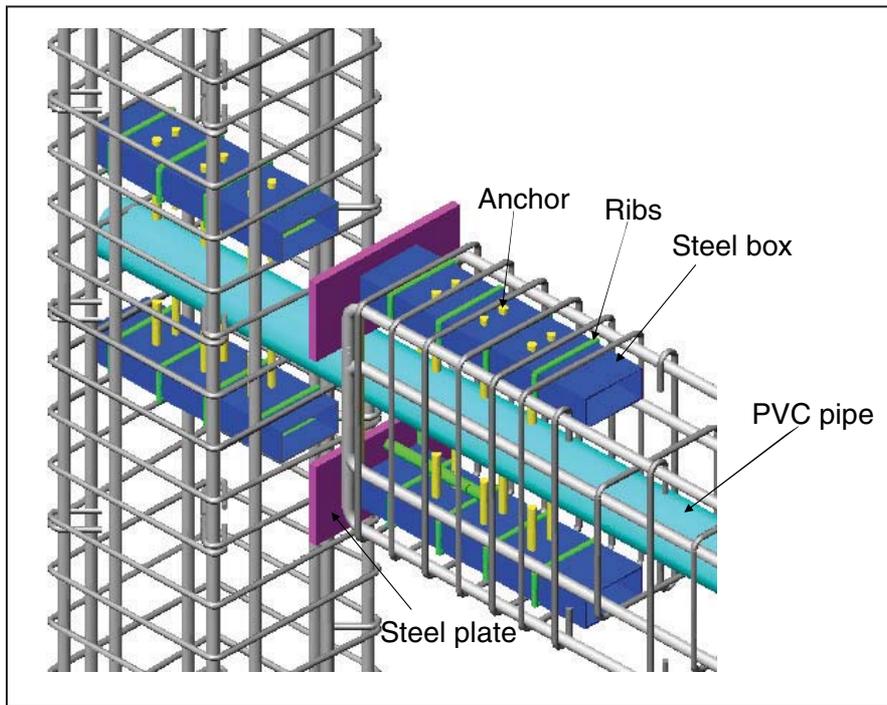
Fig. 3. Connection detail of post-tensioned specimens. Note: PVC = polyvinyl chloride.

and post-tensioned. The net effective force was measured using a load cell located at the end of the beam, and force was monitored throughout the test (**Fig. 5**). The unbonded length of the tendons was approximately 8.9 ft (2.7 m).

Specimen PTM0—The geometry and reinforcement detailing of specimen PTM0 was slightly different from that of the other post-tensioned, precast

concrete specimens. Specimen PTM0 did not have blockout channels at the top and bottom because no mild steel reinforcement was used in the connection region. Dimensions of the specimen were the same as those for the monolithic subassembly. Six 0.5-in.-diameter (13 mm) prestressing strands were located at mid-depth of the beam.

The effective post-tensioning force
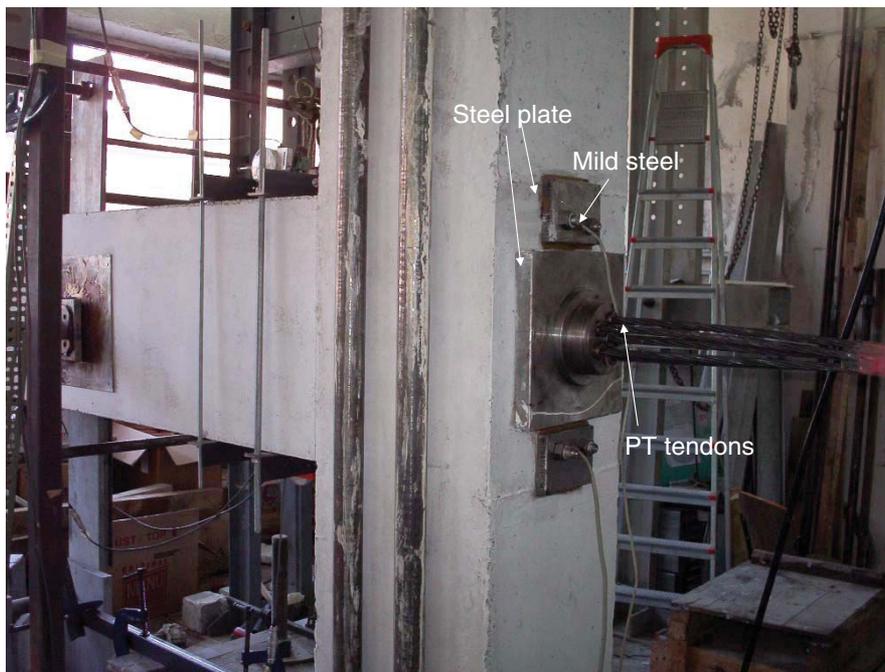
was approximately 40% of the ultimate strand strength, according to the recommendations given in ACI T1.2-03. This force resulted in a 435 psi (3 MPa) normal stress at the beam-to-column interface. Two 0.8-in.-diameter (20 mm) reinforcing bars were placed at the top and bottom of the precast concrete beam for flexural reinforcement. The measured compressive strength of the precast concrete elements was 8702 psi (60 MPa).

Specimen PTM10—Detailing of this specimen limited the contribution of mild steel reinforcement to the flexural capacity to 10%. There was one 0.4-in.-diameter (10 mm) mild steel reinforcing bar inserted at the top and the bottom of the connection with a 1.97 in. (50 mm) unbonded length, which was about five times the bar diameter. The concrete cover thickness for this reinforcing steel was 2.6 in. (65 mm). Post-tensioning was applied using six 0.5-in.-diameter (13 mm) tendons, and a 435 psi (3 MPa) normal stress was created at the beam-to-column interface. The concrete compressive strength of the precast members was 9718 psi (67 MPa).

Specimen PTM30—The post-tensioning force created by the prestressing strands in this specimen was the same as that created in PTM0 and PTM10. In order to increase the contribution of mild steel reinforcement to the flexural capacity of the connection, one 0.8-in.-diameter (20 mm) reinforcing bar was located at the top and the bottom of the cross section through the steel boxes. The concrete cover thickness was 2.45 in. (62 mm), and the unbonded length of the mild steel reinforcement in the connection region was 3.15 in. (80 mm), about four times the bar diameter. Concrete compressive strength of the precast members was 7542 psi (52 MPa).

Specimen PTM50—Two 0.8-in.-diameter (20 mm) reinforcing bars were located at the top and the bottom of the beam cross section to increase the contribution of the mild steel to 50% of the flexural strength of connection. The post-tensioning force in specimen PTM50 was the same as that of previous specimens. The unbonded length of the mild steel reinforcement was 3.15 in. (80 mm), and the measured

Fig. 4. Assembled post-tensioned connection. Note: PT = post-tensioning.

concrete compressive strength was 7542 psi (52 MPa). Cover thickness over the mild steel was about 2.36 in. (60 mm).

Specimen PTM65—Two 0.8-in.-diameter (20 mm) reinforcing bars with a 3.15 in. (80 mm) unbonded length were installed in the connection as in specimen PTM50. Three 0.5-in.-diameter (13 mm) strands were placed at mid-depth of the beam, and the post-tensioning force was about 40% of ultimate tendon strength, resulting in a 218 psi (1.5 MPa) normal stress at the beam-to-column interface. Concrete cover thickness for the mild steel was 2.6 in. (66 mm), and the concrete compressive strength for the precast members was 6237 psi (43 MPa).

Fig. 5. Test setup and instrumentation. Note: 1 ft = 0.3048 m.

TESTING PROCEDURE

The test setup was specifically designed to apply a reversed-cyclic loading procedure and the drift controlled loading scheme specified in ACI T1.1[19] (Fig. 5). The column was supported by a pinned connection at its base, and the top of the column was free to move and rotate. The beam end was designed (modeled) as a roller support. Hence, the predetermined point of contraflexure for both the beam and column was achieved within the test setup. A constant axial load was applied to the column by using a closed frame and a hydraulic ram (Fig. 5). The level of axial load on the column was 10% of its compressive capacity.

After the application of the column axial load, the lateral load history was applied through the column top (**Fig. 6**). The loading pattern followed that of ACI T1.1, and the first cycles (0.15% and 0.20% story drift) were in the elastic range. Three fully reversed cycles were applied at each story drift level, and 39 reversed cycles were conducted throughout the test. Cracks were monitored at the end of each three-cycle interval. All test specimens were loaded up to a 4% interstory drift ratio; maximum drift was due to the limited stroke capacity of the hydraulic actuator.

Linear variable displacement transducers (LVDTs) were mounted on the test specimens to measure the story drift, joint rotation, gap opening, beam curvature, and sliding of the precast concrete beam relative to the precast concrete column (Fig. 5). The net displacement at the column top Δ_{cnet} was calculated by subtracting the column base lateral displacement and the vertical beam end displacement from the lateral displacement measurement obtained from the column top.

Top displacement of the column Δ_{ct} was measured using two 7.9-in.-capacity (200 mm) LVDTs mounted at the level of the hydraulic actuator. Column base displacement Δ_{cb} was measured at the pinned support. (At a pinned support in an ideal case, lateral displacement readings should equal zero.) Vertical displacement Δ_{bv} of the beam end should equal zero for an ideal test configuration.

Displacement readings were monitored continuously, and the net column displacement was calculated according to Eq. 1, where a 6.3:5.9 ratio was used due to geometric compatibility (the column height was 6.3 ft [1.9 m], and the beam span was 5.9 ft [1.8 m]). Consequently, story drift values were calculated as Δ_{cnet}/6.3 ft. A load cell was installed at the end of the beam to measure the initial effective post-tensioning force. By using this load cell, average stress changes in the prestressing strands were monitored during the cyclic loading.

$$A_{cnet} = \Delta_{ct} - \Delta_{cb} - \left[\frac{6.3}{5.9} \left(\Delta_{bv} \right) \right] \qquad (1)$$
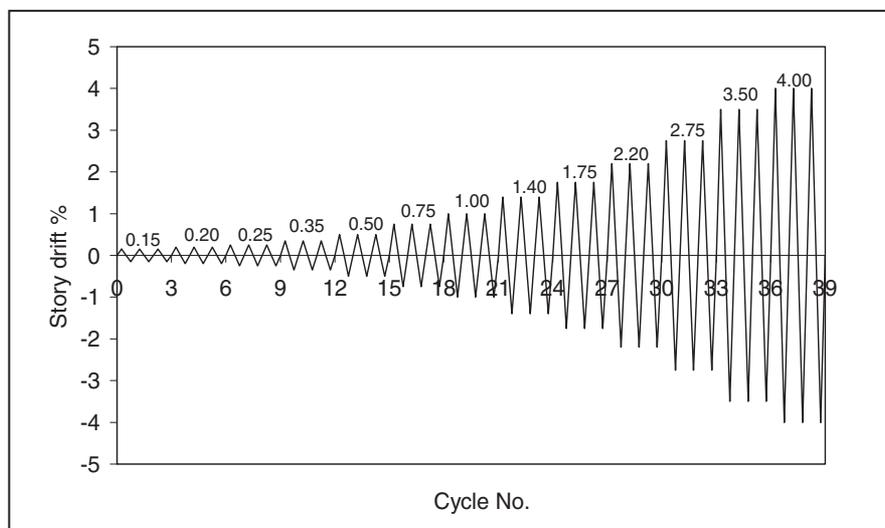
Fig. 6. Loading history.

Fig. 7. Damage in monolithic specimen M at 4% drift level.

TEST RESULTS

Monolithic Specimen

The response of specimen M was nearly elastic during the first two successive loading cycles. At the 0.25% story drift level, minor flexural cracks were observed on the beam at a distance of 10 in. (250 mm) from the column face. Hairline diagonal cracks at the joint core appeared at the 0.75%

story drift level. The 1.0% story drift cycle was approximately the yielding load level for the mild steel reinforcement.

The first diagonal crack in the beam was observed at a distance of 31.5 in. (800 mm) from the column surface at the 1.4% story drift level. Spalling of the beam concrete at the joined end started at 3.5% drift level, and the beam top flexural reinforcing bars buckled at 4% story drift (**Fig. 7**). Cracks were

well distributed over the beam at the joined end region.

The hysteretic behavior of specimen M is shown in **Fig. 8**. The ultimate loads for the forward and backward cycles measured 25.6 kip (114 kN) and -33.5 kip (-149 kN), respectively. Specimen M underwent no significant strength degradation or pinching effect until reaching the 4% story drift level. In general, the behavior of specimen M was acceptable in terms of ductility and energy dissipation.

Post-Tensioned Specimens

The post-tensioned, precast concrete connections had predetermined crack locations at the beam-to-column interface because of the imposed cold joints. During the load cycles, a predetermined crack opening/closing type of response was observed in the connection region and minor cracks were observed on the precast concrete beams and columns. Specimens PTM0, PTM10, and PTM30 behaved as self-centering systems, while the behaviors of specimens PTM50 and PTM65 were similar to that of specimen M.

Specimen PTM0—No flexural or diagonal cracks were observed in the specimen until the 0.35% story drift cycle. At this level, a hairline crack was initiated at the beam-to-column in-

Fig. 8. Lateral load versus story drift response of monolithic specimen M.

Fig. 9. Damage in specimen PTM0 at the 4% drift level.

terface and this crack widened with increasing story drift levels. No cracking or crushing was observed in the precast concrete elements at the 4% story drift level (**Fig. 9**).

At the end of the test, there were no visible cracks or residual displacement in the subassembly. The behavior of specimen PTM0 was like a bilinear spring (**Fig. 10**). The maximum lateral load was 20.7 kip (92 kN) for forward and -20.0 kip (-89 kN) for reverse cycles. Also, the average maximum stress σ_{ave} in the strands was measured as 65% of the ultimate capacity throughout the loading history.

Specimen PTM10—The first visible crack in this specimen was observed at the 0.25% story drift level at the beam-to-column interface. At the 0.75% story drift, a flexural crack was observed near the blockout channel and strain gauges indicated yielding of the mild steel reinforcement at the connection. The 0.4-in.-diameter (10 mm) mild steel reinforcing bars at the connection were ruptured at the 2.2% story drift cycle due to insufficient unbonded length. There was no indication of bond deterioration near the 0.4-in.-diameter steel bars at the end of test.

After the rupture of the mild steel reinforcement, the behavior of specimen PTM10 was more like that of specimen PTM0. The effect of the small amount of mild steel reinforcement content was minor for the overall hysteretic behavior (**Fig. 11**). The maximum load for forward and reverse cycles was 21.8 kip (97 kN) and -22.7 kip (-101 kN), respectively, and the maximum average stress σ_{ave} in the prestressing tendons was 68% of their ultimate capacity. The residual displacement at the end of the test was less than 0.04 in. (1 mm). The crack pattern of specimen PTM10 at the 4% story drift level is shown in **Fig. 12**.

Specimen PTM30—When the contribution of mild steel reinforcement to the flexural capacity was increased, the load-versus-story-drift response of the test specimen was improved (**Fig. 13**). Mild steel was the dominant factor affecting the hysteretic loops at high drifts, and residual displacement was negligible. At the 4% story drift level (**Fig. 14**), a 0.28 in. (7 mm) permanent displacement was observed. The
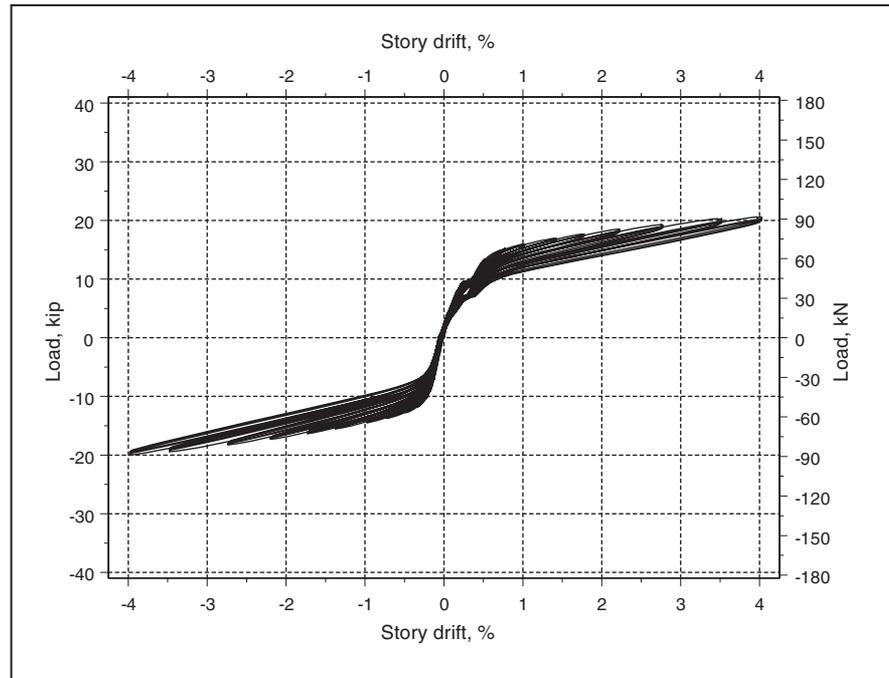
Fig. 10. Lateral load versus story drift response of specimen PTM0.
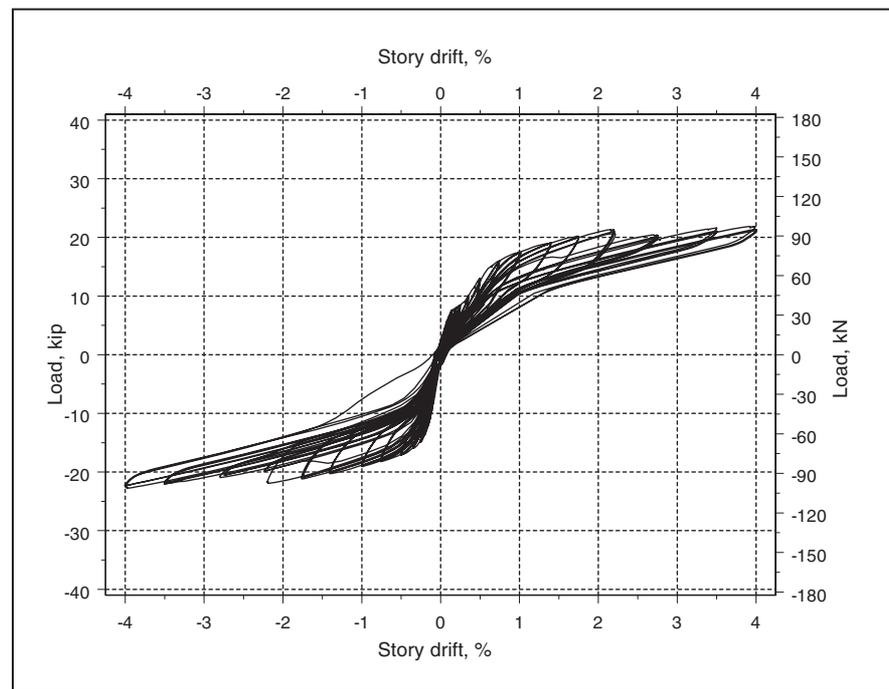
Fig. 11. Lateral load versus story drift response of specimen PTM10.

maximum lateral loads were 27.9 kip (124 kN) and -29.9 kip (-133 kN) for forward and reverse loadings, respectively. The prestressing tendons attained 63% of ultimate capacity, indicating an elastic response. A minor flexural crack on the beam was observed about 20 in. (500 mm) from the column face at the 0.75% story drift level.

Specimen PTM50—Minor flexural cracks were observed at mid-length of the precast concrete beam at the 0.5% story drift level. The mild steel reinforcing bars yielded at the 0.75% drift cycle. The first diagonal crack at the joint core was observed at the 3.5% story drift level. The crack distribution at the 4% story drift level is shown in **Fig. 15**. The hysteretic behavior of specimen PTM50 approached that of

Fig. 12. Damage in specimen PTM10 at the 4% drift level.

specimen M (**Fig. 16**). The maximum measured lateral load was 35.5 kip (158 kN) for the forward cycle and -38.8 kip (-173 kN) for the reverse cycle. The maximum average stress σ_{ave} in the prestressing strands was 60% of the ultimate value, and the residual displacement was 1.38 in. (35 mm). This permanent displacement was greater than the expected value despite the fact that the mild steel reinforcement content was within the limits recommended by ACI T1.2-03.

Specimen PTM65—Hairline cracks

appeared at the blockout channel location on the precast concrete beam at the 0.5% story drift level. Top mild steel reinforcing bars at the connection were ruptured at the second and third cycles of the 4% story drift level. **Figure 17** shows the crack distribution at the 4% story drift level. The response of specimen PTM65 was similar to that of specimen M (**Fig. 18**), and this response may be due to the high content of mild steel reinforcement. The permanent displacement was 1.97 in. (50 mm), and the measured maximum lateral loads were 26.3 kip (117 kN) and -27.9 kip (-124 kN) for forward and reverse cycles, respectively. The tendons were loaded up to 63% (σ_{ave}) of their ultimate strength at the 4% story drift load cycles.

Evaluation of Test Results

The experimental capacities of the post-tensioned test specimens were compared with the capacity predictions based on ACI T1.2-03 design procedures. Stiffness degradation, energy dissipation characteristics, and residual displacements of the hybrid specimens were compared with those of the monolithic specimen, and these comparisons are presented in the following sections.

Strength—Plastic moment capacities and ultimate stress values in the

prestressing tendons for each post-tensioned connection were calculated according to ACI T1.2-03 at the 4% story drift level. True prediction of the gap opening in calculations of flexural strength of the connection was of prime importance. Therefore, the coefficient of the effective additional debonded length α_s was chosen accordingly. Although this coefficient was proposed to be 5.5 by Cheok et al.,[20] Raynor et al.[21] recommended a value of $\alpha_s = 2$ for the same mild steel reinforcement properties. In the design of the precast concrete specimens, the $\alpha_s = 3$ was chosen for the current research. It was observed
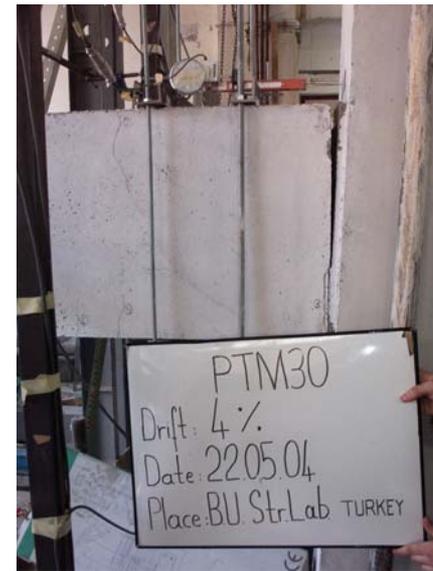
Fig. 14. Damage in specimen PTM30 at the 4% drift level.

Fig. 15. Damage in specimen PTM50 at the 4% drift level.
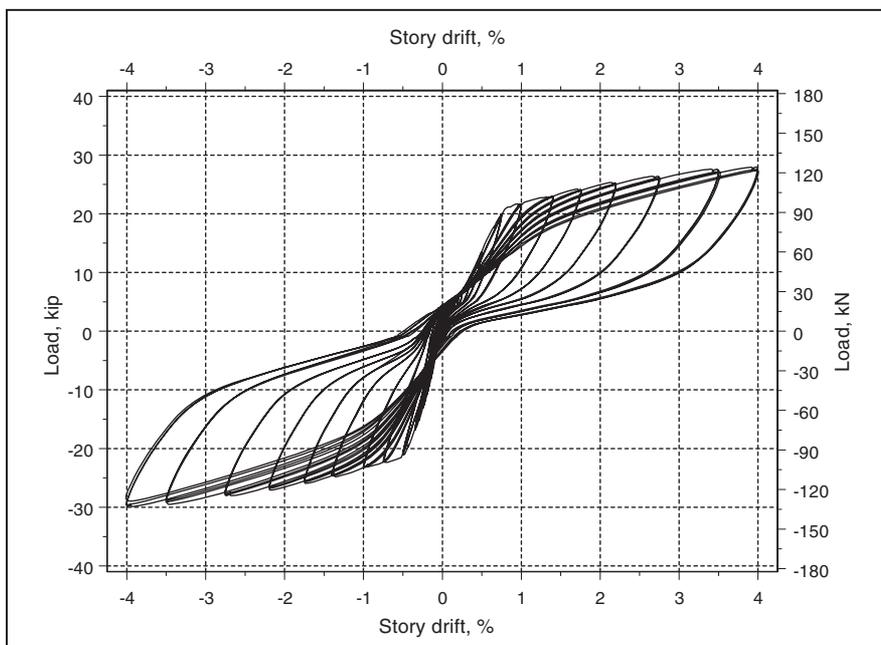
**Fig. 13.** Lateral load versus story drift response of specimen PTM30.
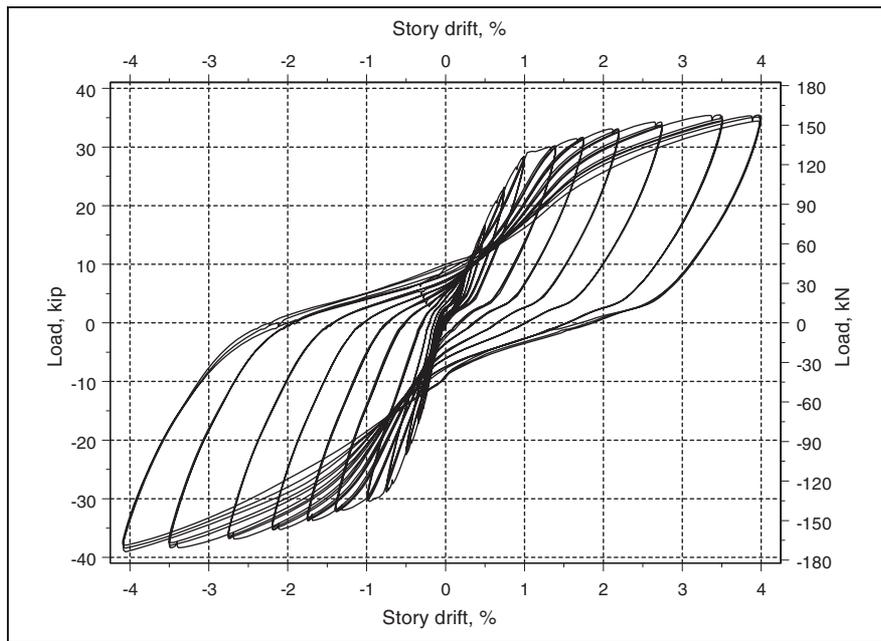
Fig. 16. Lateral load versus story drift response of specimen PTM50.

in experiments that $\alpha_s = 3$ yielded the best predictions for the phase II specimens. Table 1 lists predicted capacities, test results, and the experimental over-calculated ratios.

Because the amount of top and bottom mild steel reinforcement at the connection was equal in each specimen, the experimental flexural strength M_{ave} and stress in the prestressing strands σ_{ave} were determined by taking the average value of the forward and reverse cycle

at the 4% story drift level. Strength predictions are believed to be very important in defining the connection performance in terms of lateral load capacity. All tested connection types reached the calculated flexural ultimate moment capacity. Note in Table 1 that experimental results for the moment capacity were greater, by about 5%, than the calculated values M_{cal}, indicating that all connections had adequate capacity. This result may be related to the

existence of steel plates located on the cross-sectional surface of the beam at the connection region and may be a result of the confining effect of the closed stirrups (located in the beam close to the connection region).

Stress prediction values in the prestressing strands σ_{cal} were very close to experimental results for specimens PTM0, PTM10, and PTM30. Conversely, the estimation of stress in tendons was greater than the measured values for specimens PTM50 and PTM65. These results may be due to the behavior of the hybrid connection in approaching that of the monolithic subassembly (with increasing mild steel reinforcement content and the resulting permanent displacements). The relation between the story drift angle and the gap-opening angle measured on the beam-to-column interface is linear until the load at which the beam body starts cracking. This relation is important for capacity calculations as defined by Cheok et al.

Stiffness Degradation—Secant stiffness K_{sec} calculated on the last cycle for each successive story drift level was used to compare stiffness degradation among the test specimens. The secant stiffness was defined as the slope of the straight line connecting the maximum drift levels of that specific load cycle. As shown in **Fig. 19**, K_{sec} is also

Fig. 17. Damage in specimen PTM65 at the 4% drift level.
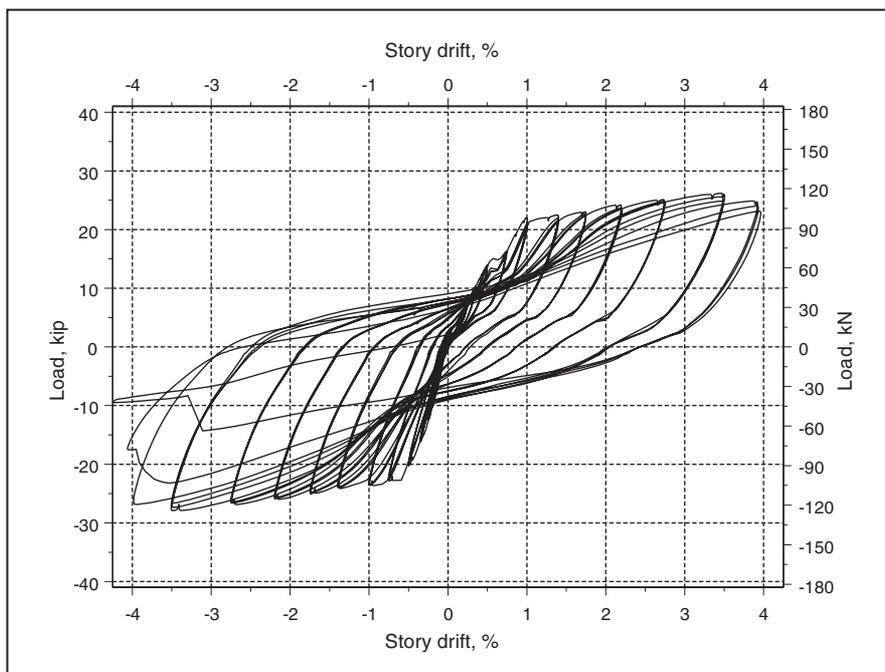
Fig. 18. Lateral load versus story drift response of specimen PTM65.
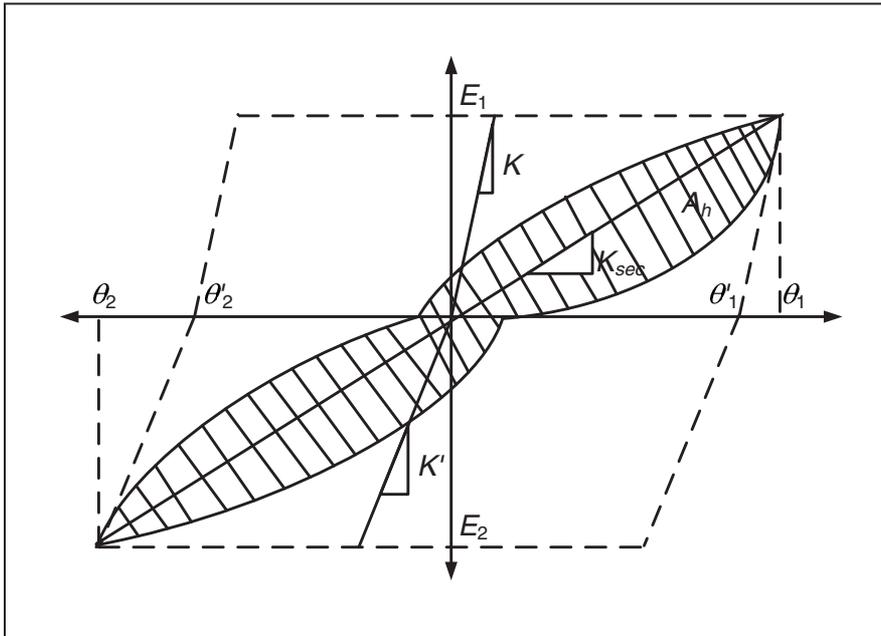
Fig. 19. Illustration of secant stiffness and relative energy dissipation ratio.
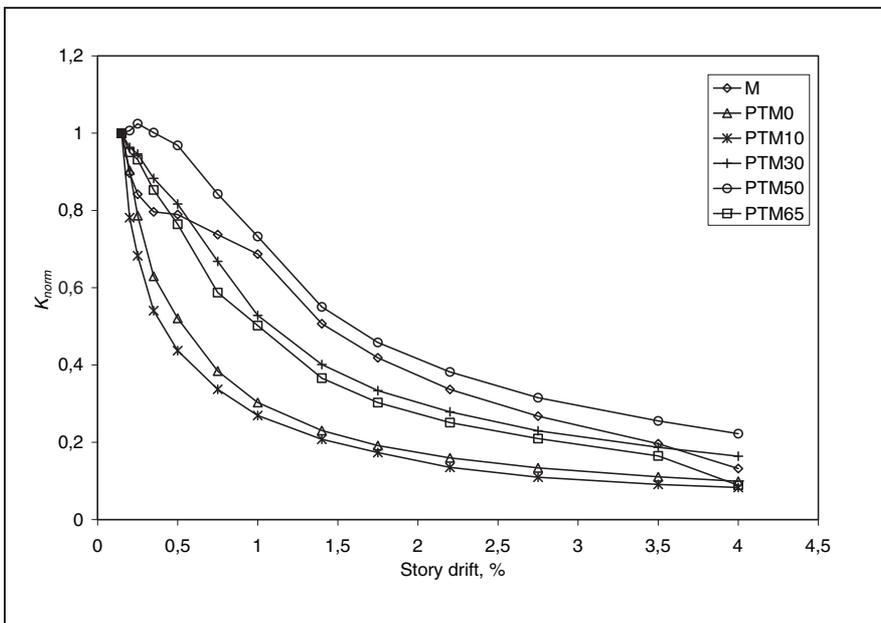
Fig. 20. Stiffness degradation of specimens.

named the peak-to-peak stiffness. Each secant stiffness value was normalized K_{norm} with respect to the secant stiffness measured at the 0.15% story drift level for a possible comparison among the phase II specimens. The use of normalized secant stiffness has the advantage of easy comparison with other test specimens and avoids subjective assumptions.

Figure 20 presents the stiffness degradation of the monolithic and post-tensioned test specimens. The secant stiffness of the post-tensioned specimens was significantly degraded as the gap opened at the beam-to-column interface. The stiffnesses of specimens PTM0 and PTM10 decreased greatly, with a loss of stiffness at the 4% drift level of approximately 90%. Therefore, displacement-based methodology may be a more rational design approach for such connections.[22] With the addition of mild steel reinforcement to the connection, the stiffness degradation behavior changed, approaching that of the monolithic specimen M.

Energy Dissipation—In order to highlight the energy dissipation characteristics of the test specimens, the relative energy dissipation ratio β was plotted against the story drift level (**Fig. 21**). The energy dissipation concept is defined in ACI T1.1-01 as an acceptance criterion for such subassemblies (Fig. 19). The dissipated energy can be measured as the hatched area A_h in the third cycle of a given story drift level. Normalization of this value is assessed with respect to the elasto-plastic behavior of the specimen at this specified load cycle.

The initial stiffness (K and K') values and peak loads (E_1 and E_2) may be

Table 1. Test Results and Predictions

Test Specimen	Experimental		Calculated		Ratio	
	1	2	3	4	5	6
	M_{ave}, kip-in.	$\sigma_{ave}/\sigma_{ult}$, %	M_{cal}, kip-in.	$\sigma_{cal}/\sigma_{ult}$, %	(1)/(3)	(2)/(4)
PTM0	1537	65	1452	66	1.06	0.98
PTM10	1692	68	1617	66	1.05	1.03
PTM30	2191	63	2014	65	1.09	0.97
PTM50	2824	60	2620	64	1.08	0.94
PTM65	2051	63	1970	68	1.04	0.93

Note: 1 kip-in. = 0.113 kN-m.
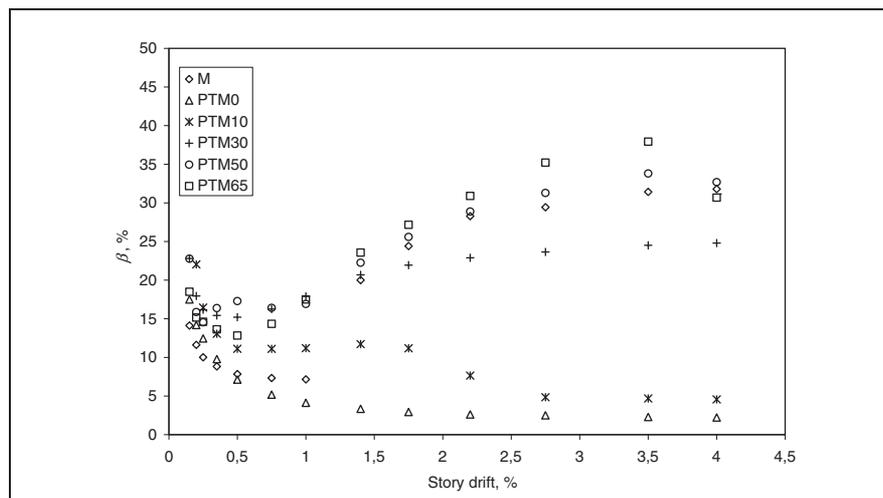
Fig. 21. The relative energy dissipation ratios versus story drift response.

different for the forward and reverse cycles when the specimen is exhibiting elasto-plastic behavior. The relative energy dissipation ratio is defined as the hatched area divided by the area of the effective circumscribing parallelograms.[19] This ratio definition β is formulated and given in Eq. (2). As an acceptance criterion according to ACI T1.1-01, the relative energy dissipation ratio of a subassembly must be equal to or exceed $\frac{1}{8}$ of the value of the third cycle at the 3.5% story drift level.

$$\beta(\%) = \frac{A_h}{(E_1 + E_2)(\theta_1' + \theta_2')}(100) \quad (2)$$

It was observed that the relative energy dissipation ratio increases with an increasing story drift level, as shown in **Fig. 21**, except for specimens PTM0 and PTM10. The energy dissipation characteristics of specimens PTM50 and PTM65 were similar to the monolithic specimen at higher drift levels. On the other hand, specimens PTM0 and PTM10 had widely different characteristics compared with specimen M. The energy dissipation of specimen PTM10 increased up to the point of rupture of the mild steel reinforcement at the connection. After rupture, specimen behavior was very similar to that of specimen PTM0. At the 2% story drift level, which may be adopted as a possible design level, β values were in the range of 2% to 7% for specimens PTM0 and PTM10, while β values reached up to 20% to 25% for specimens PTM50 and PTM65.

The behavior of specimen PTM30 could be categorized as being between that of other specimens in terms of energy dissipation performance. Furthermore, specimens PTM30, PTM50, and PTM65 satisfied the acceptance criteria for the relative energy dissipation ratio at the 3.5% story drift level according to ACI T1.1-01. The calculated β values for these test modules exceeded the $\frac{1}{8}$ value noted previously. It may be concluded that a mild steel reinforcement contribution for flexural strength of about 20% to 30% may be an adequate range for creating a damping effect on the post-tensioned, precast concrete structures.

Residual Displacement—Post-tensioned, precast concrete connections are typically designed as self-centering systems. For hybrid systems, the moment-resisting frame is

expected to exhibit minimal damage in beam-to-column connection region and negligible residual displacements after a major seismic event.[3] **Figure 22** plots the residual displacement data of the test specimens. Up to a 30% mild steel reinforcement contribution to the flexural moment capacity, the permanent displacement was negligible. At the 4% story drift level, a 0.28 in. (7 mm) residual displacement was recorded for specimen PTM30. Prior to yielding of the mild steel reinforcement in specimens PTM50 and PTM65, the residual displacements were minor. After the reinforcement yielding point, permanent displacements reached 1.4 in. to 2.0 in. (35 mm to 50 mm) at the end of the test.

CONCLUSIONS

Based on test results presented here and from the observations during the tests, the following conclusions may be drawn:

- All post-tensioned, precast concrete specimens have adequate flexural strength that can be sustained up to a 4% story drift without major strength degradation. Calculation of flexural strength and stress in the prestressing strands according to ACI T1.2-03 generally coincided with the experimental results. In addition, test results showed that the assumption of $\alpha_s = 3$ is rational.
- The hysteretic behavior of the hybrid connections approached
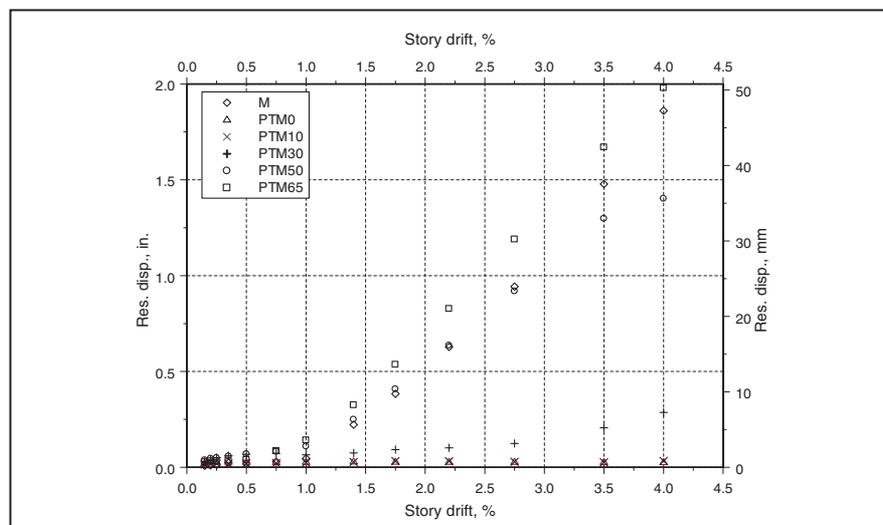
Fig. 22. Residual displacements at the subassembly depending on the story drift.

that of the monolithic specimen with increasing mild steel reinforcement content, exhibiting very small or negligible damage to the precast concrete beam and column.

- The value of secant stiffness changed significantly with the opening of the precracked interface in the hybrid subassembly. Therefore, displacement-based design methodology may be more reasonable for seismic design of hybrid precast concrete frames.
- The energy dissipation characteristics of specimens PTM50 and PTM65 are very similar to those of the monolithic specimen. On the other hand, specimens PTM0 and PTM10 did not satisfy the energy dissipation criteria at 3.5% story drift according to ACI T1.1-01.
- Test results indicated that permanent displacement depends on the contribution of mild steel reinforcement to the moment capacity. Up to a 30% mild steel reinforcement contribution for flexural strength, residual displacements are negligible. Permanent displacements for specimens PTM50 and PTM65 reached about 1.4 in. to 2.0 in. (35 mm to 50 mm).
- A 20% to 30% mild steel reinforcement contribution to the flexural strength seems to be the most rational connection design, if adequate strength, ductility, relative energy dissipation ratio, and minimum permanent displacement criteria are considered.

REFERENCES

1. Englekirk, R. E. 1990. Seismic Design Consideration for Precast Concrete Multistory Buildings. *PCI Journal*, V. 35, No. 3 (May–June): pp. 40–51.

2. Ertas, O., S. Ozden, and T. Ozturan. 2006. Ductile Connections in Precast Concrete Moment Resisting Frames. *PCI Journal*. V. 51, No. 3 (May–June): pp. 66–76.

3. ACI Innovation Task Group 1 and Collaborators. 2003. *Special Hybrid Moment Frames Composed of Discretely Jointed Precast and Post-Tensioned Concrete Members (T1.2-03) and Commentary (T1.2R-03)*. American Concrete Institute. Farmington Hills, MI: ACI.

4. Park, R., and K. Thompson. 1977. Cyclic Load Test on Prestressed and Partially Prestressed Beam-Column Joints. *PCI Journal,* V. 22, No. 5 (September–October): pp. 84–110.

5. Thompson, K., and R. Park. 1980. Ductility of Prestressed and Partially Prestressed Concrete Beam Sections. *PCI Journal,* V. 25, No. 2 (March–April): pp. 47–69.

6. French, C. W., O. Amu, and C. Tarzikhan. 1989. Connections between Precast Elements Failure outside Connection Region. *Journal of Structural Engineering,* V. 115, No. 2 (February): pp. 316–340.

7. French, C. W., M. Hafner, and V. Jayashankar. 1989. Connection between Precast Elements—Failure within Connection Region. *Journal of Structural Engineering*, V. 115, No. 12 (December): pp. 3171–3192: American Society of Civil Engineers.

8. Palmieri, L., E. Saqan, C. French, and M. Kreger. 1996. Ductile Connections for Precast Concrete Frame Systems. *Mete A. Sozen Symposium—A Tribute from His Students*. SP 162-13, pp. 313–355. Farmington Hills, MI: ACI.

9. Cheok, G. S., and H. S. Lew. 1991. Performance of Precast Concrete Beam-to-Column Connections Subject to Cyclic Loading. *PCI Journal,* V. 36, No. 3 (May–June): pp. 57–67.

10. Cheok, G. S., and W. C. Stone. 1993. *Performance of 1/3 Scale Model Precast Concrete Beam-Column Connections Subjected to Cyclic Inelastic Loads*. Report NIST IR 5246-3. National Institute for Standards and Technology (NIST).

11. Priestley, M. J., and J. R. Tao. 1993. Seismic Response of Precast Prestressed Concrete Frames with Partially Debonded Tendons. *PCI Journal,* V. 38, No. 1 (January–February): pp. 58–69.

12. Stone, W. C., G. S. Cheok, and J. F. Stanton. 1995. Performance of Hybrid Moment-Resisting Precast Beam-to-Column Concrete Connections Subjected to Cyclic Loading. *ACI Structural Journal,* V. 91, No. 2 (March–April): pp. 229–249.

13. Priestley, M. J., and G. A. MacRae. 1996. Seismic Tests of Precast Beam-to-Column Joint Subassemblages with Unbonded Tendons. *PCI Journal*, V. 41, No. 1 (January–February): pp. 64–80.

14. Priestley, M. J. 1991. Overview of PRESSS Research Program. *PCI Journal,* V. 36, No. 4 (July–August): pp. 50–57.

15. Nakaki, S. D., J. F. Stanton., and S. Sritharan. 1999. An Overview of the PRESSS Five-Story Precast Test Building. *PCI Journal,* V. 44, No. 2 (March–April): pp. 26–39.

16. Priestley, M. J. N., S. Sritharan, J. Conley, and S. Pampanin. 1999. Preliminary Results and Conclusions from the PRESSS Five-Story Precast Concrete Test Building. *PCI Journal*, V. 44, No. 6 (November–December): pp. 42–67.

17. Turkish Standards Institute. 1979. *Building Code Requirements for Prestressed Concrete* (*TS3233*).

18. Ministry of Public Works and Settlement. 1998. *Specifications for Structures to Be Built in Disaster Areas*. Ankara, Turkey: Ministry of Public Works and Settlement.

19. ACI Innovation Task Group 1 and Collaborators and ACI Committee 374. 2001. *T1.1-01/T1.1R-01: Acceptance Criteria for Moment Frames Based on Structural Testing*. Farmington Hills, MI: ACI.

20. Cheok, G. S., W. C. Stone, and S. D. Nakaki. 1996. *Simplified Design Procedure for Hybrid Precast Concrete Connections*. Report NIST IR 5765. NIST.

21. Raynor, D. J., D. E. Lehman, and J. F. Stanton. 2002. Bond-Slip Response of Reinforcing Bars Grouted in Ducts. *ACI Structural Journal,* V. 99, No. 5 (September–October): pp. 568–576.

22. Stanton, J., W. C. Stone, and G. S. Cheok. 1997. A Hybrid Reinforced Precast Frame for Seismic Regions. *PCI Journal*, V. 42, No. 2 (March–April): pp. 20–32.

Resources   About   News & Events   Publications   Foundation   Education

Members   Find

PCI Journal - Issue Archives

Home

Home > Publications > PCI Journal

This is a back issue of journal. Use the links below
file of the story you wish to see. If you do not hav
Reader you can download one here.

March-April 2007 TOC

<< Next Issue   mar-apr   2007   Previous Issue >>

Chuanbing Sun, Shane Hennessey, Mark Ahlman, and Maher Tadros
JL-07-MARCH-APRIL-8.PDF - 840.3 KB PDF FILE

Effectiveness of Continuity Diaphragm for Skewed Continuous Prestressed Bridges
Aziz Saber, Freddy Roberts, Walid Alaywan, and Joseph Toups
JL-07-MARCH-APRIL-9.PDF - 500.0 KB PDF FILE

Prediction of Long-Term Prestress Losses
Samer Youakim, Amin Ghali, Susan Hida, and Vistasp Karbhari
JL-07-MARCH-APRIL-10.PDF - 755.8 KB PDF FILE

Project Study
Budweiser of Greenville Warehouse and Distribution Center, Piedmont, South Ca
JL-07-MARCH-APRIL-11.PDF - 448.7 KB PDF FILE

Chairman's Message
Robert Konoske
JL-07-MARCH-APRIL-12.PDF - 83.1 KB PDF FILE

Editor's Message
Emily Lorenz
JL-07-MARCH-APRIL-13.PDF - 828.6 KB PDF FILE

Letters
Letters
JL-07-MARCH-APRIL-14.PDF - 154.8 KB PDF FILE

Reference Cards
Reference Cards
JL-07-MARCH-APRIL-15.PDF - 119.3 KB PDF FILE

Abstracts of Technical Publications
Tech Abstracts
JL-07-MARCH-APRIL-16.PDF - 91.2 KB PDF FILE

Industry News
Industry News
JL-07-MARCH-APRIL-17.PDF - 779.0 KB PDF FILE

JPCI Journal

Precast/Prestressed Concrete Institute

CONNE
CONNEC
CONNECT
OURNAL
NNECTIO
NECTION
ECTIONS
CTIONS
TIONS
IONS